ACS NANO
Cite This: ACS Nano 2019, 13, 9993−10001
www.acsnano.org

ARTICLE

Clear Wood toward High-Performance Building Materials

Chao Jia,[†,¶] Chaoji Chen,[†,¶] Ruiyu Mi,[†,¶] Tian Li,[†] Jiaqi Dai,[†] Zhi Yang,[‡] Yong Pei,[‡] Shuaiming He,[†] Huiyang Bian,[§] Soo-Hwan Jang,[†] J. Y. Zhu,[§] Bao Yang,[‡] and Liangbing Hu*[,†]

[†]Department of Materials Science and Engineering, University of Maryland College Park, College Park, Maryland 20742, United States

[‡]Department of Mechanical Engineering, University of Maryland, College Park, Maryland 20742, United States

[§]Forest Products Laboratory, USDA Forest Service, Madison, Wisconsin 53726, United States

Supporting Information

ABSTRACT: **Developing advanced building materials with both excellent thermal insulating and optical properties to replace common glass (thermal conductivity of ~1 W m^{-1} K^{-1}) is highly desirable for energy-efficient applications. The recent development of transparent wood suggests a promising building material with many advantages, including high optical transmittance, tunable optical haze, and excellent thermal insulation. However, previous transparent wood materials generally have a high haze (typically greater than 40%), which is a major obstacle for their practical application in the replacement of glass. In this work, we fabricate a clear wood material with an optical transmittance as high as 90% and record-low haze of 10% using a delignification and polymer infiltration method. The significant removal of wood components results in a highly porous microstructure, much thinner wood cell walls, and large voids among the cellulose fibrils, which a polymer can easily enter, leading to the dense structure of the clear wood. The separated cellulose fibrils that result from the removal of the wood components dramatically weaken light scattering in the clear wood, which combined with the highly dense structure produces both high transmittance and extremely low haze. In addition, the clear wood exhibits an excellent thermal insulation property with a low thermal conductivity of 0.35 W m^{-1} K^{-1} (one-third of ordinary glass); thus, the application of clear wood can greatly improve the energy efficiency of buildings. The developed clear wood, combining excellent thermal insulating and optical properties, represents an attractive alternative to common glass toward energy-efficient buildings.**

KEYWORDS: *building materials, wood nanocomposites, thermal insulation, clear, cellulose nanomaterials*

The energy consumed for lighting and regulating indoor temperature in residential and commercial buildings accounts for approximately 40% of the total global energy consumption, which is more than that amount consumed by the industrial and transportation sectors.[1,2] Tremendous efforts have been devoted to reducing indoor energy consumption, mainly through advancements in personal thermal management[3−8] and building cooling technologies.[9−14] Common glass, as an important building material, has a critical impact on indoor energy consumption. Generally, glass possesses high total light transmittance, allowing natural light to enter structures and reduce the use of artificial light. However, glass exhibits a relatively high thermal conductivity (~1 W m^{-1} K^{-1}), which results in high heat loss and low energy efficiency.[15] Therefore, it is urgent to improve the thermal insulation of glass or develop alternative transparent materials with both excellent thermal insulating and optical properties to be used as a replacement.[15−17]

Transparent wood is a promising building material and has shown many advantages, including high optical transmittance, tunable optical haze, excellent thermal insulation, high impact energy absorption, and great potential for functionalization.[15,17−25] Although the haze of transparent wood can be adjusted, it still typically exceeds 40%, making it a challenge to prepare transparent wood with sufficiently low haze to rival common glass. For example, our group obtained transparent wood by removing lignin in basswood using a boiling solution of sodium hydroxide (NaOH) and sodium sulphite (Na_2SO_3)

Received: January 4, 2019
Accepted: August 13, 2019
Published: September 10, 2019

DOI: 10.1021/acsnano.9b00089
ACS Nano 2019, 13, 9993−10001

and subsequent hydrogen peroxide (H_2O_2) treatment, followed by infiltration with epoxy.[18] The resulting transparent wood possessed high transmittance (79.4%) but high haze (88.7%) at a wavelength of 550 nm. Berglund and co-workers prepared transparent wood by delignification of natural balsa wood using sodium chlorite ($NaClO_2$) and infiltration of poly(methyl methacrylate) (PMMA).[19] At a thickness of 0.7 mm, their transparent wood demonstrated a transmittance of 91.7% and a haze of 48.9% at 550 nm. Tiwari and co-workers removed lignin in natural beech wood using a $NaClO_2$ solution followed by PMMA infiltration.[20] At a thickness of 0.7 mm, the transparent wood showed a low transmittance of 13.0% and a high haze of 49.3% at 550 nm. Despite these tremendous efforts, the simultaneous achievement of high transmittance and ultralow haze remains a huge challenge in the development of sustainably sourced wood-based glass alternatives.

In this work, we developed a transparent wood composite (named as clear wood) with both high transmittance (90%) and record-low haze (10%) in the visible spectrum by mildly removing lignin and hemicellulose from natural wood and infiltrating it with an epoxy resin (Figure 1). During

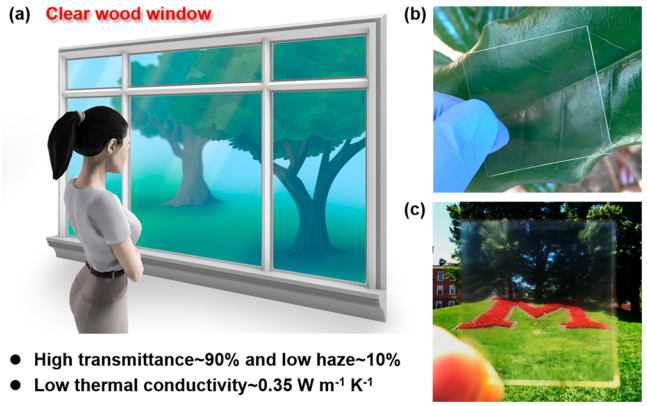

Figure 1. Schematic illustration of the clear wood and its digital images. (a) Schematic demonstrating how clear wood can be used as a building material, particularly clear wood windows. (b,c) Digital images show the clear wood has high transmittance and very low haze. Photos: Chao Jia.

delignification, almost all lignin and some hemicellulose materials were removed, and the delignified wood can be easily decomposed into cellulose nanomaterials by vigorous shaking, which is totally different from the delignified wood obtained by previous delignification processes.[17−20,22] After delignification, the wood structure becomes more porous and the cell walls become much thinner (from ∼4 μm for the original wood to ∼1.5 μm for the delignified wood), while the aligned microchannels (lumens) are well preserved. The infiltration of epoxy into the delignified wood creates a dense structure, which together with the separated cellulose fibrils due to voids among them resulting from the removal of the wood components dramatically weakens light scattering in the clear wood, resulting in both high transmittance and ultralow haze. In addition, the clear wood possesses a very low thermal conductivity of 0.35 W m^{-1} K^{-1}, which is much lower than that of common glass. The excellent thermal insulating and optical properties of the clear wood make it a potential building material for energy-efficient applications.

RESULTS AND DISCUSSION

We obtained original basswood samples with a thickness of ∼0.7 mm by cutting a tree trunk along the tree growth direction (Figure 2a). The wood samples exhibit a yellowish color due to the presence of light-absorbing lignin (Figure S1). Uneven pores and highly aligned microchannels can be observed from the cross-sectional and top views of the original wood film, respectively (Figures S2−S4). The original wood is opaque because of light scattering at the interfaces between air and the microchannels/cell walls.

In order to obtain clear wood, we first carefully removed lignin from the original wood to reduce the light absorption (Figure 2a). The original basswood is mainly composed of 42.70% cellulose, 18.14% hemicellulose, and 22.34% lignin (Figure 2b). The delignification process was performed by immersing the original wood film in NaClO solution until it was completely bleached. The delignification process caused a noticeable increase in the relative content of cellulose, while the content of hemicellulose and lignin was significantly decreased (Figures 2b and S5). In particular, the content of lignin dramatically reduced to 1.60% after the NaClO treatment, suggesting the almost complete removal of lignin. After delignification, the wood structures become more porous and the cell walls become much thinner (from ∼4 μm for the original wood to ∼1.5 μm for the delignified wood, Figures 2c−g, S3 and S6), while the aligned microchannels are well preserved (Figures 2e and S7).

In order to obtain the clear wood with high transmittance and low haze, we infiltrated clear epoxy resin into the NaClO-delignified wood framework (Figure 2a). Note that the epoxy has a density of 1.08 g cm^{-3} and a refractive index of 1.55 at the wavelength of 550 nm (Figure S8). Scanning electron microscopy (SEM) images demonstrate that the microchannels in the NaClO-delignified wood are fully filled with the resin (Figures 2f−h). Note that the volume fraction of cellulose in the clear wood is only 2.54%. In addition, aligned cellulose nanofibers can be observed in the high-magnification SEM image of the wood structure, indicating the wood microstructures are maintained (Figure 2i). The dense structure is one reason why our clear wood demonstrates both high transmittance and low haze.

After delignification, the container with NaClO-delignified wood was vigorously shaken, and a suspension of cellulose nanomaterial was obtained and analyzed. We measured the morphology and height of the cellulose nanomaterial using atomic force microscopy (AFM), as shown in Figures 2j,k. The cellulose nanomaterials possess a height of ∼2.5 nm (Figure 2k), which is similar to that of cellulose nanofibers prepared by TEMPO-mediated oxidation or cellulose nanocrystals from acid hydrolysis.[26−29] The acquisition of cellulose nanomaterials demonstrated that the cellulose fibrils were well separated by voids resulting from the significant removal of the wood components. When infiltrated with epoxy, the separated cellulose fibrils can dramatically weaken light scattering in the clear wood, resulting in high transmittance and ultralow haze.

Compared with NaClO-delignified wood, the $NaClO_2$-delignified wood cannot be decomposed into cellulose nanomaterials by vigorous shaking, demonstrating the strong interaction between cellulose fibrils (Figure S9). This phenomenon can be ascribed to the reduced removal of wood components. Note that the yield of the $NaClO_2$-

DOI: 10.1021/acsnano.9b00089
ACS Nano 2019, 13, 9993−10001

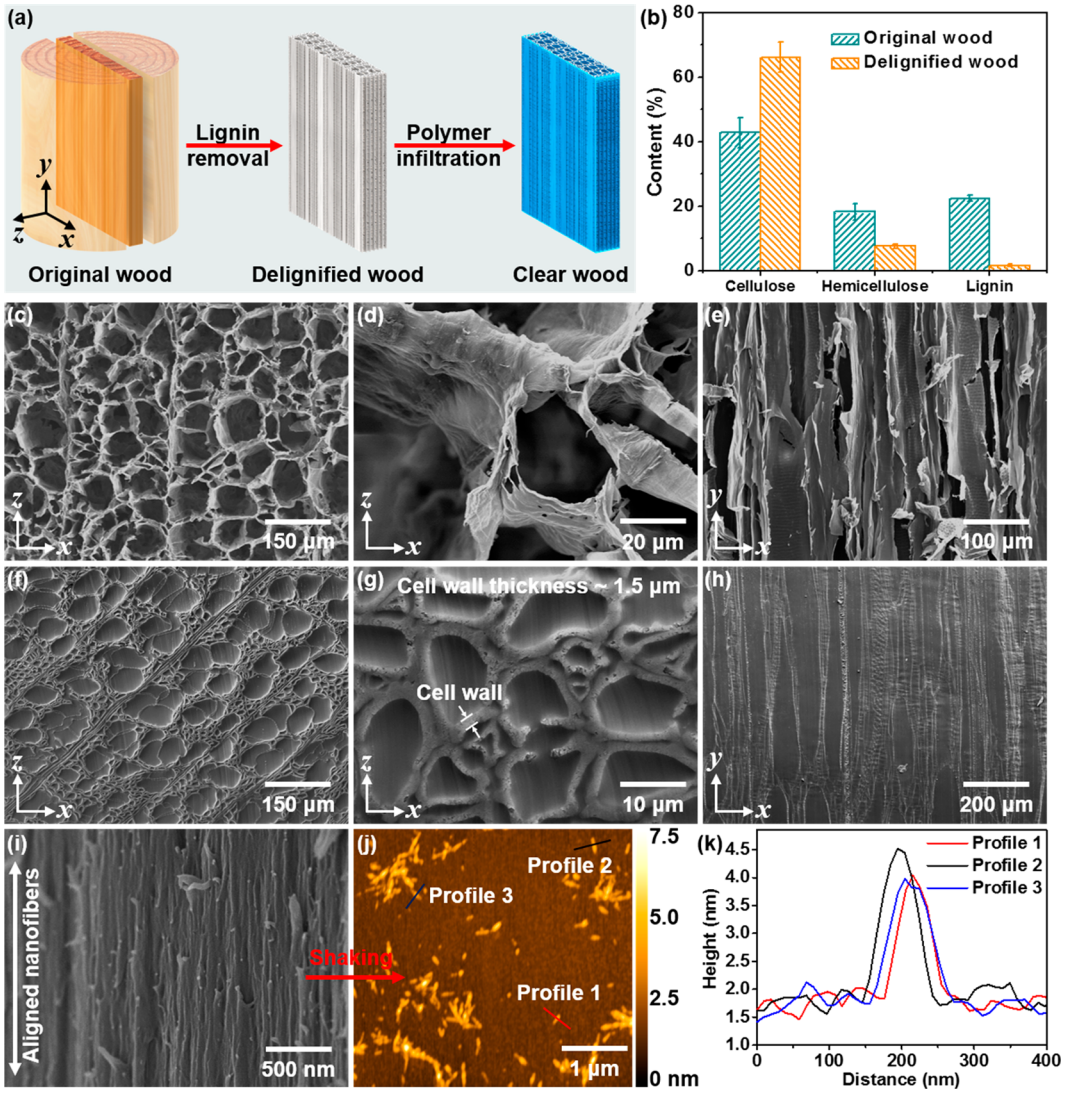

Figure 2. Microstructure characterization of the NaClO-delignified wood and clear wood. (a) Schematic demonstrating the preparation process of the clear wood, which includes two steps: delignification and polymer infiltration. (b) Cellulose, hemicellulose, and lignin content in the original wood and NaClO-delignified wood. (c) Cross-sectional SEM image of the NaClO-delignified wood. (d) Magnified cross-sectional SEM image of the delignified wood. After delignification, the wood structure becomes more porous, and the cell walls are thinner. (e) SEM image of the NaClO-delignified wood in the longitudinal direction. After delignification, the oriented microchannels are well preserved. (f) Cross-sectional SEM image of the clear wood. (g) Magnified cross-sectional SEM image of the clear wood. (h) SEM image of the clear wood longitudinal direction. (i) Magnified SEM image of the clear wood longitudinal direction to show the aligned cellulose nanofibers. (j) AFM topography image of the cellulose nanomaterials obtained by vigorously shaking the container with NaClO-delignified wood. (k) Typical heights of the cellulose nanomaterials.

delignified wood is as high as 76.09%, while the yield of NaClO-delignified wood is only 16.37%, indicating a large amount of the initial cellulose is removed during the NaClO delignification process.

We determined the total transmittance and haze of the clear wood using a UV−vis spectrophotometer with an integrating sphere over the wavelength range of 400−800 nm. The principle for the determination of total transmittance and haze can be found in previous publications.[21,30,31] The total transmittance refers to the percentage of the transmitted light collected at all angles using an integrating sphere, while the optical haze refers to the percentage of the forward light scattering. Our clear wood exhibits transmittance as high as 90% and ultralow haze of just ~10% (Figure 3a). For comparison, we also fabricated transparent wood (named as haze wood) using $NaClO_2$-delignified wood as the template and measured its optical properties (Figure 3b). It is important to note that $NaClO_2$-delignified wood has been widely used to prepare transparent wood in recent publications.[19,32,33] Haze wood possesses a total transmittance of ~90% (similar to that of clear wood), but it also demonstrates a very high haze of ~80%. These optical properties are demonstrated in the insets of Figures 3a,b, in which we can clearly see the words on the background through the clear wood, while the words become blurred through the haze wood. Compared with $NaClO_2$-delignified wood, the NaClO-delignified wood shows a lower yield, indicating that more wood components are removed during the delignification process. Therefore, the NaClO-delignified wood possesses more voids, and the cellulose fibrils become small enough (Figure 2j). The small cellulose fibrils scattered less light and resulted in a low haze.[30]

DOI: 10.1021/acsnano.9b00089
ACS Nano 2019, 13, 9993−10001

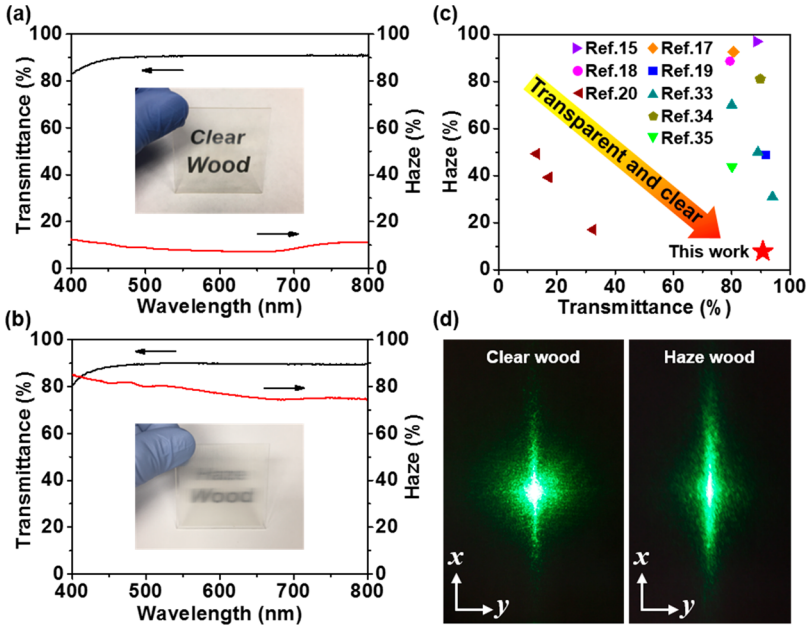

Figure 3. Optical properties of the clear wood and haze wood. (a) Optical transmittance and haze of the clear wood. The inset is a digital image of the clear wood to show its high transmittance and low haze. (b) Optical transmittance and haze of the haze wood prepared using $NaClO_2$-delignified wood. The inset is a digital image of the haze wood to show its high haze. (c) Optical haze versus transmittance of our clear wood and other transparent wood materials made from different preparation processes and wood species.[15,17−20,33−35] The optical properties at a wavelength of 550 nm were used for comparison. (d) The light scattering patterns of the transmitted light through the clear wood (left) and haze wood (right).

We obtained transparent wood with different wood volume fractions by regulating the delignification time. When the wood volume fraction increased from 2.89% to 5.86%, the transmittance and haze did not show obvious change. However, the haze significantly increased to 41.6% at 550 nm wavelength when the wood volume fraction of the transparent wood increased to 8.71%, which can be ascribed to the increased number of scattering centers (Figure S10a). In addition, we also found that the thickness has a significant effect on the optical properties of the transparent wood. The transmittance reduced to 84.9% and the haze significantly increased to 40.1% at 550 nm wavelength when the thickness increased from 0.7 mm to 1.5 mm, which can be attributed to the longer light pathway and increased scattering centers (Figure S10b).

We evaluated the UV stability of our clear wood by exposing them to sunlight for 3 weeks, and we determined their transmittance and haze. Compared with the original clear wood (Figure 3a), the sunlight-exposed clear wood became slightly yellow (Figure S11). After being exposed to sunlight, the transmittance of the clear wood decreased slightly in the wavelength range of 400−500 nm, while no obvious change was observed in the wavelength range of 500−800 nm (Figure S12). The change in transmittance is difficult to visualize from the appearance of the clear wood (Figure S11a). In addition, the optical haze of the clear wood increased from 10.1% to 15.0% at the wavelength of 550 nm after 3 weeks sunlight exposure (Figure S12e), which may have occurred because of the color change of the clear wood. These results suggest that the UV stability of the clear wood should be further improved to make this material an excellent candidate to replace common glass.

Compared with other transparent wood from different preparation processes and wood species, the haze of our clear wood is among the lowest (Figure 3c and Table S1).[15,17−20,33−35] We ascribe the high transmittance and ultralow haze of the clear wood to the following reasons. First, the NaClO-delignified wood possesses a highly porous microstructure, much thinner cell walls, and large voids among the cellulose fibrils compared with the original wood, which allows the epoxy to easily enter the voids of the cell walls and among the cellulose fibrils, leading to a dense structure. Note that the void volume fraction of the clear wood is only 0.26%, which is much smaller than that of the haze wood (haze wood has a void volume fraction of 4.44%). Second, the NaClO-delignified wood shows a very low yield, and more wood components are removed, indicating that more voids are generated during the delignification process. The separated small cellulose fibrils dramatically weaken light scattering in the clear wood, thus resulting in the high transmittance and ultralow haze. Last but not the least, the cellulose volume fraction in the clear wood is only 2.54%, which is much lower than that of other transparent wood (Table S2). The low cellulose content results in the reduced number of scattering centers, which is also an important reason for the low haze of our clear wood.

We also obtained the light scattering patterns of the clear wood and haze wood, and we quantified the anisotropy of the x−y scattering, as shown in Figures 3d and S13. The samples were vertically irradiated by a single mode green laser featuring a spot size of around 200 μm. The haze wood demonstrates a highly anisotropic light scattering effect, and a smaller refractive index variation in the y direction is observed (Figure S13a), which can be ascribed to the anisotropic microstructure and densely stacked aligned cellulose fibrils. In contrast, the light scattering and scattered light intensity distribution in the x and y directions are similar for our clear wood, and the scattering angle is significantly reduced (Figure S13b),

DOI: 10.1021/acsnano.9b00089
ACS Nano 2019, 13, 9993−10001

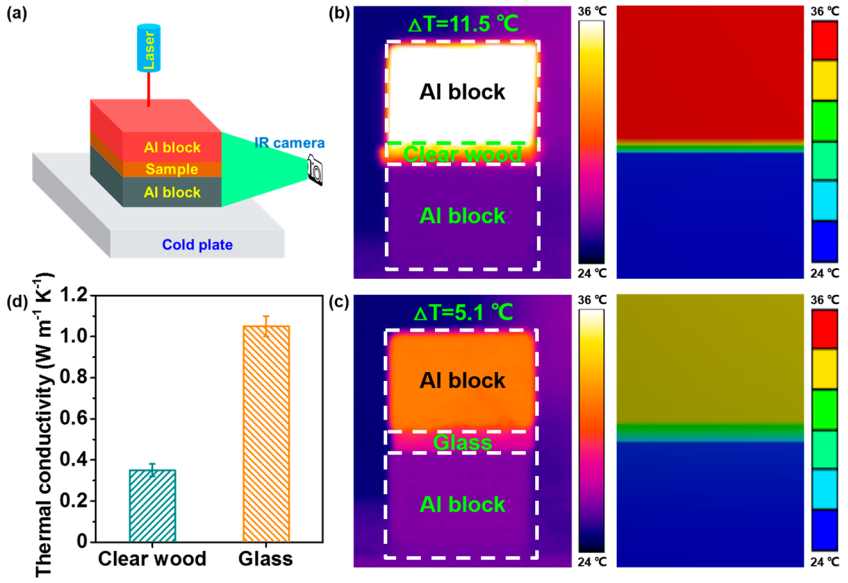

Figure 4. Thermal conductivity of the clear wood and common glass. (a) Schematic to show the thermal conductivity measurement system. (b) Infrared image of the clear wood to show the temperature distribution at a given heating power input (left) and the temperature distribution result obtained by ANSYS numerical simulation (right). (c) Infrared image of common glass to show the temperature distribution at a given heating power input (left) and the temperature distribution result obtained by ANSYS numerical simulation (right). (d) Thermal conductivities of the clear wood and common glass.

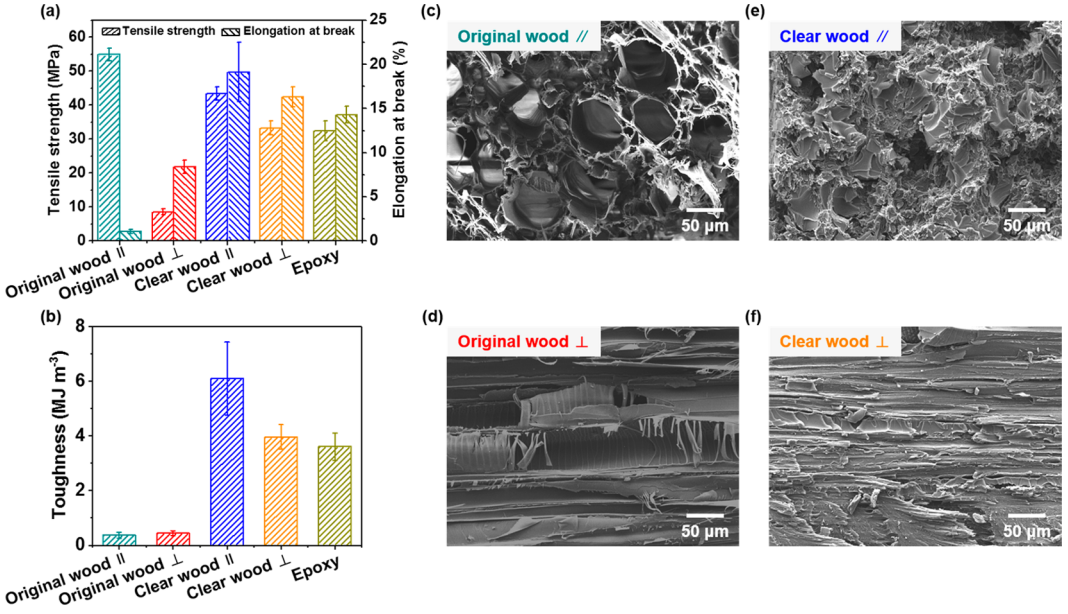

Figure 5. Mechanical properties of the original wood, clear wood and epoxy. (a) Tensile strength and elongation at break of the original wood, clear wood and epoxy. Note that the ∥ symbol denotes the applied stress parallel to the wood channel direction and the ⊥ symbol denotes the applied stress vertical to the wood channel direction. (b) Toughness of the original wood, clear wood and epoxy. (c-d) SEM images of the fracture surface of the original wood after tensile testing at different directions. (e,f) SEM images of the fracture surface of the clear wood after tensile testing at different directions.

indicating reduced light scattering resulting from the separated cellulose fibrils.

The use of building materials with excellent thermal insulation properties is crucial for saving energy because they can effectively block heat flow into or out of a building and improve energy efficiency.[36−38] Therefore, low thermal conductivity is highly desirable for practical building applications. We investigated the thermal conductivity of the clear wood and compared it with common glass. The thermal conductivities of the clear wood and glass were measured with a steady-state laser-infrared camera thermal-conductivity-characterization system, which consists of a laser heat source, two standard aluminum (Al) blocks, a water-cooled cold plate, and an infrared thermal camera (Figure 4a). The samples were placed between the two highly conductive Al blocks (206 W m^{-1} K^{-1}), and the laser (Coherent Highlight FAP-1000, 820 nm) was used to heat up the top Al block. The steady-state temperature distribution was recorded using a FLIR Merlin MID Infrared (IR) camera. The temperature differences (ΔT) between the top and bottom surfaces of the clear wood and

DOI: 10.1021/acsnano.9b00089
ACS Nano 2019, 13, 9993−10001

glass were 11.5 and 5.1 °C, respectively, and their thermal conductivities were 0.35 and 1.05 W m^{-1} K^{-1}, obtained by combining the experimental results with ANSYS numerical simulations based on the temperature differences (Figures 4b–d).[39] We attribute the lower thermal conductivity of the clear wood to the large thermal interfacial resistance and multiple interface phonon scattering effect across the wood cell walls.[15] These results confirmed that our clear wood is an excellent thermal insulation material and can be a candidate for energy-efficient buildings.

In addition, we also determined the thermal conductivity of the haze wood using the same method (Figure S14). The haze wood possesses a thermal conductivity of 0.24 W m^{-1} K^{-1}, which is slightly lower than that of the clear wood. The lower thermal conductivity of the haze wood can be ascribed to the less infiltration of epoxy resin resulted from the less removal of wood components. Because the bulk epoxy resin has a higher thermal conductivity of 0.43 W m^{-1} K^{-1} (Figure S15) than the original basswood,[15,40] the less infiltration of epoxy resin in the haze wood leads to a lower thermal conductivity. The haze wood with excellent thermal insulation and high haze can be a potential candidate for energy-efficient building applications where maintaining indoor privacy is preferred. Compared with haze wood, the prepared clear wood possesses not only similar thermal conductivity and light transmittance but also much lower haze, which enables the clear wood to be an attractive alternative to common glass toward energy-efficient buildings.

We investigated the mechanical properties of the original wood and clear wood at different tensile directions to determine the applicability of our clear wood for construction purposes (Figures 5a and S16). The tensile strength of the original wood∥ (applied stress parallel to the wood channel direction) and original wood⊥ (applied stress vertical to the wood channel direction) was 54.88 and 8.50 MPa, respectively, and the elongation values at break were 1.07% and 8.37%. The small elongation at break of the original wood∥ and the small tensile strength of the original wood⊥ lead to low toughness, with values of 0.37 and 0.44 MJ m^{-3}, respectively (Figure 5b). Compared with the original wood⊥, the elongation at break of the clear wood⊥ increased to 16.30%, and the tensile strength significantly enhanced to 33.29 MPa, resulting in a significantly improved toughness of 3.96 MJ m^{-3}—about 8-times higher than the original wood⊥. We attribute the improved mechanical properties of the clear wood⊥ to the reinforcement effect of the epoxy (note that the tensile strength and elongation at break of the epoxy are 32.44 MPa and 14.30%, respectively). For the clear wood∥, although its tensile strength decreased to 43.39 MPa, the elongation at break increased to 19.14%; thus, a toughness as high as 6.10 MJ m^{-3} was obtained.

We also determined the mechanical properties of the clear wood after 3 weeks of sunlight exposure to evaluate the effects of sunlight on the mechanical properties of the clear wood (Figure S17). There is no significant degradation in the mechanical properties for our clear wood, and the change extent for all the mechanical properties, including tensile strength, elongation at break, and toughness is less than 13%, indicating that sunlight has no significant effect on the mechanical properties of the clear wood in a short period of time (e.g., 3 weeks). Compared with transparent wood made from other preparation processes and wood species,[15,18,33] our clear wood shows much higher toughness, indicating it possesses a higher ductility, which can be attributed to the nanoscale structure of the wood framework (Figure S18 and Table S2). In addition, glass possesses a very low toughness of 0.1 MJ m^{-3}, demonstrating its inherent brittleness.[33] The significant high ductility of the clear wood is highly desirable in the field of building materials.

We carefully examined the fracture surfaces of the original wood and clear wood after the tensile tests using SEM (Figures 5c–f). The original wood possesses a porous structure with highly oriented microchannels. After the tensile test, the uneven pores and aligned microchannels can be clearly seen in the fracture surfaces of the original wood∥ and original wood⊥, respectively (Figures 5c,d). In contrast, the fracture surfaces of the clear wood∥ and clear wood⊥ exhibit a very dense structure and are relatively smooth due to the infiltration of epoxy (Figures 5e,f). Since the breakage happens between the microchannels for original wood⊥ and clear wood⊥ and less interaction exists between the microchannels, the original wood⊥ and clear wood⊥ demonstrate lower mechanical strength (Figure 5a). On the other hand, the aligned microstructure results in higher mechanical strength for original wood∥ and clear wood∥.

CONCLUSIONS

In summary, we have developed a clear wood composite featuring excellent thermal insulating and optical properties by removing wood components from natural wood and infiltrating polymer in the delignified wood. The clear wood exhibited a high transmittance of 90% and record-low haze of 10%, which is comparable to common glass. To the best of our knowledge, the haze of our clear wood is the lowest of all transparent wood composites. The excellent optical properties can be ascribed to the separated cellulose fibrils due to voids among them in the delignified wood, the very dense structure of the clear wood, and the reduced number of scattering centers resulted from the low cellulose content, which is enabled by our developed delignification and infiltration method. In addition, our clear wood has demonstrated a low thermal conductivity of 0.35 W m^{-1} K^{-1}, which is one-third of that found in common glass. Compared with transparent wood made from other preparation processes, our clear wood possesses much higher toughness and ductility. The excellent optical properties, low thermal conductivity, and good mechanical properties position clear wood as a potential building material, whose application could greatly improve the energy efficiency of residential and commercial buildings.

Finally, we have to admit that the combination of favorable optical properties with high mechanical properties is a difficult challenge, and the mechanical properties need to be sacrificed for improved optical properties. In addition, the environmental and UV stability of the clear wood have not been fully characterized in our work, and the life cycle assessment should also be evaluated in order to apply the clear wood in real situations for energy saving. The UV stability of the clear wood should be further improved, and only when all the UV stability issues are solved can the clear wood be an excellent candidate to replace common glass.

EXPERIMENTAL SECTION

Materials and Chemicals. Basswood blocks with a density of 454.74 ± 23.35 kg m^{-3} were purchased from Walnut Hollow Company. Sodium hypochlorite (NaClO) solution (5%, Laboratory grade) was provided by Carolina Biological Supply Company. Sodium chlorite ($NaClO_2$, 80%) and acetic acid were purchased from Sigma-

DOI: 10.1021/acsnano.9b00089
ACS Nano 2019, 13, 9993–10001

Aldrich. Epoxy resin (#300 resin and #21 Non Blushing Cycloaliphatic Hardener, AeroMarine Products, Inc.) was used for infiltration. Ethanol and deionized (DI) water were used to wash the delignified wood.

Preparation of Delignified Wood. The wood films (cutting along the longitudinal direction) were put in 5% NaClO solution, and the delignification process proceeded at room temperature. When the wood films were bleached completely (about 72 h of bleaching), they were washed using 50% ethanol solution several times to remove the residual NaClO solution. The density of the NaClO-delignified wood for clear wood preparation is 93.41 ± 17.01 kg m^{-3}.

A 5% $NaClO_2$ solution was obtained by adding $NaClO_2$ powder in DI water, and the pH value was adjusted to about 4.6 by adding acetic acid in the $NaClO_2$ solution. The delignified wood used for haze wood fabrication was obtained by immersing the wood films in boiling $NaClO_2$ solution until the samples became completely white (about 2 h of bleaching). After that, the samples were washed using 50% ethanol solution several times to remove any residual chemicals.[41] The density of the $NaClO_2$-delignified wood for haze wood preparation is 345.92 ± 15.46 kg m^{-3}. The $NaClO_2$-delignified wood was composed of 63.54 ± 2.85% cellulose, 15.16 ± 0.88% hemicellulose, and 1.24 ± 0.46% lignin.

Fabrication of Clear Wood and Haze Wood. The two components of epoxy resin (#300 resin and #21 non blushing cycloaliphatic hardener) were premixed at a weight ratio of 2:1. The clear wood and haze wood samples were fabricated by immersing the delignified wood in epoxy resin under vacuum for about 15 min to fully infiltrate the samples. Then the clear wood and haze wood samples were dried at ambient temperature until the epoxy resin was fully cured. The clear wood has a density of 1.09 ± 0.02 g cm^{-3}, and the haze wood has a density of 1.11 ± 0.04 g cm^{-3}.

Characterization. The morphologies of the wood samples were characterized using a field emission scanning electron microscope (FESEM, HITACHI SU-70). The compositional analysis of the wood samples was performed according to previous research.[42] The morphology of the cellulose nanomaterials was observed by atomic force microscopy (AFM) (Dimension FastScan, Bruker Corporation) in tapping mode. The mechanical properties of the samples were measured using a tensile tester (Instron). Four samples were used for each determination, and the averages were presented. The transmittance and haze were characterized by a UV−vis spectrophotometer equipped with an integrating sphere (Lambda 35, PerkinElmer, U.S.A.). Light-scattering measurements were performed using our previous method.[43] The thermal conductivities were measured using a steady state laser-infrared camera thermal conductivity characterization system, as described previously.[39] The volume fraction of cellulose or wood material in the clear wood and haze wood was calculated according to the following equations: $\varphi_c\ (\%) = \frac{V_c}{V_{cw}} \times 100\%$; $V_c = \frac{m_{dw} \times \omega_c}{\rho_c}$, where φ_c is the volume fraction of cellulose or wood material in the clear wood and haze wood, V_c is the volume of cellulose or wood material in the clear wood and haze wood, V_{cw} is the volume of the clear wood and haze wood, m_{dw} is the mass of delignified wood, ω_c is the mass fraction of cellulose or wood material in the delignified wood, ρ_c is the density of cellulose or wood material (ρ_c = 1.5 g cm^{-3}). (Here wood material includes cellulose, hemicellulose, and lignin.) The void volume fraction in the transparent wood was calculated according to the following equations: $\varphi_v\ (\%) = (1 - \varphi_c - \varphi_e) \times 100\%$; $\varphi_e\ (\%) = \frac{\rho_t - \rho_c \times \varphi_c}{\rho_e} \times 100\%$, where φ_v is the void volume fraction in the clear wood and haze wood, φ_c is the volume fraction of delignified wood, φ_e is the volume fraction of epoxy, ρ_t is the density of clear wood and haze wood, ρ_c is the density of wood material (ρ_c = 1.5 g cm^{-3}), ρ_e is the density of epoxy (ρ_e = 1.08 g cm^{-3}). Three samples were used for the determination of the volume fraction of cellulose or wood material in the clear wood and haze wood, and the average was presented. The refractive index of the epoxy was measured using an ellipsometer in the wavelength range of 400−800 nm (Uvisel, Horiba scientific, France).

ASSOCIATED CONTENT

Supporting Information

The Supporting Information is available free of charge on the ACS Publications website at DOI: 10.1021/acsnano.9b00089.

Digital image and SEM images of the original wood; relative content of cellulose, hemicellulose, and lignin in the original wood, NaClO-delignified wood, and $NaClO_2$-delignified wood; SEM images of the NaClO-delignified wood; refractive index of the epoxy in the wavelength range of 400−800 nm; digital images of the $NaClO_2$-delignified wood; optical and mechanical properties of the clear wood and other transparent wood materials made from different preparation processes and wood species; optical property of the clear wood with different wood volume fraction and thickness; UV stability of the clear wood; scattered light intensity distribution of the clear wood and haze wood; infrared images of the haze wood and epoxy; stress−strain curves of the original wood, clear wood, and haze wood; optical images and mechanical properties of the clear wood after 3 weeks sunlight exposure (PDF)

AUTHOR INFORMATION

Corresponding Author

*E-mail: binghu@umd.edu.

ORCID

Chaoji Chen: 0000-0001-9553-554X

Liangbing Hu: 0000-0002-9456-9315

Author Contributions

¶C.J., C.C., and R.M. contributed equally to this work. L.H. and C.J. initiated the concept. C.J., R.M., and S.H. carried out the preparation of the clear wood and haze wood. C.C. did the SEM characterization. Z.Y., Y.P., and B.Y. performed the thermal conductivity measurements. H.B. and J.Z. did the wood composition analysis. C.J. and T.L. determined the optical properties. C.J. measured the mechanical properties. S.J. performed the AFM characterization. J.D. drew the schematics. L.H., C.J., and C.C. collaboratively analyzed all the data and wrote the manuscript. All authors commented on the manuscript.

Notes

The authors declare no competing financial interest.

ACKNOWLEDGMENTS

The authors acknowledge support of the A. James & Alice B. Clark Foundation and the A. James School of Engineering at the University of Maryland.

REFERENCES

(1) Nejat, P.; Jomehzadeh, F.; Taheri, M. M.; Gohari, M.; Abd. Majid, M. Z. A Global Review of Energy Consumption, CO_2 Emissions and Policy in the Residential Sector (with an Overview of the Top Ten CO_2 Emitting Countries). *Renewable Sustainable Energy Rev.* **2015**, *43*, 843−862.

(2) Perez-Lombard, L.; Ortiz, J.; Pout, C. A Review on Buildings Energy Consumption Information. *Energy Build* **2008**, *40*, 394−398.

(3) Peng, Y.; Chen, J.; Song, A. Y.; Catrysse, P. B.; Hsu, P.-C.; Cai, L.; Liu, B.; Zhu, Y.; Zhou, G.; Wu, D. S.; Lee, H. R.; Fan, S.; Cui, Y. Nanoporous Polyethylene Microfibres for Large-Scale Radiative Cooling Fabric. *Nat. Sustainability* **2018**, *1*, 105−112.

(4) Hsu, P. C.; Liu, C.; Song, A. Y.; Zhang, Z.; Peng, Y.; Xie, J.; Liu, K.; Wu, C. L.; Catrysse, P. B.; Cai, L.; Zhai, S.; Majumdar, A.; Fan, S.;

DOI: 10.1021/acsnano.9b00089
ACS Nano 2019, 13, 9993−10001

Cui, Y. A Dual-Mode Textile for Human Body Radiative Heating and Cooling. *Sci. Adv.* **2017**, *3*, No. e1700895.
(5) Hsu, P. C.; Song, A. Y.; Catrysse, P. B.; Liu, C.; Peng, Y.; Xie, J.; Fan, S.; Cui, Y. Radiative Human Body Cooling by Nanoporous Polyethylene Textile. *Science* **2016**, *353*, 1019−1023.
(6) Hsu, P. C.; Liu, X.; Liu, C.; Xie, X.; Lee, H. R.; Welch, A. J.; Zhao, T.; Cui, Y. Personal Thermal Management by Metallic Nanowire-Coated Textile. *Nano Lett.* **2015**, *15*, 365−371.
(7) Zhao, D.; Lu, X.; Fan, T.; Wu, Y. S.; Lou, L.; Wang, Q.; Fan, J.; Yang, R. Personal Thermal Management Using Portable Thermoelectrics for Potential Building Energy Saving. *Appl. Energy* **2018**, *218*, 282−291.
(8) Gao, T.; Yang, Z.; Chen, C.; Li, Y.; Fu, K.; Dai, J.; Hitz, E. M.; Xie, H.; Liu, B.; Song, J.; Yang, B.; Hu, L. Three-Dimensional Printed Thermal Regulation Textiles. *ACS Nano* **2017**, *11*, 11513−11520.
(9) Rotzetter, A. C. C.; Schumacher, C. M.; Bubenhofer, S. B.; Grass, R. N.; Gerber, L. C.; Zeltner, M.; Stark, W. J. Thermoresponsive Polymer Induced Sweating Surfaces as an Efficient Way to Passively Cool Buildings. *Adv. Mater.* **2012**, *24*, 5352−5356.
(10) Raman, A. P.; Anoma, M. A.; Zhu, L.; Rephaeli, E.; Fan, S. Passive Radiative Cooling Below Ambient Air Temperature under Direct Sunlight. *Nature* **2014**, *515*, 540−544.
(11) Synnefa, A.; Santamouris, M.; Livada, I. A Study of the Thermal Performance of Reflective Coatings for the Urban Environment. *Sol. Energy* **2006**, *80*, 968−981.
(12) Wanphen, S.; Nagano, K. Experimental Study of the Performance of Porous Materials to Moderate the Roof Surface Temperature by Its Evaporative Cooling Effect. *Build. Environ.* **2009**, *44*, 338−351.
(13) Alvarado, J. L.; Terrell, W.; Johnson, M. D. Passive Cooling Systems for Cement-Based Roofs. *Build. Environ.* **2009**, *44*, 1869−1875.
(14) Chan, H.-Y.; Riffat, S. B.; Zhu, J. Review of Passive Solar Heating and Cooling Technologies. *Renewable Sustainable Energy Rev.* **2010**, *14*, 781−789.
(15) Li, T.; Zhu, M.; Yang, Z.; Song, J.; Dai, J.; Yao, Y.; Luo, W.; Pastel, G.; Yang, B.; Hu, L. Wood Composite as an Energy Efficient Building Material: Guided Sunlight Transmittance and Effective Thermal Insulation. *Adv. Energy Mater.* **2016**, *6*, 1601122.
(16) Liu, Q.; Frazier, A. W.; Zhao, X.; De La Cruz, J. A.; Hess, A. J.; Yang, R.; Smalyukh, I. I. Flexible Transparent Aerogels as Window Retrofitting Films and Optical Elements with Tunable Birefringence. *Nano Energy* **2018**, *48*, 266−274.
(17) Yu, Z.; Yao, Y.; Yao, J.; Zhang, L.; Chen, Z.; Gao, Y.; Luo, H. Transparent Wood Containing $CsxWO_3$ Nanoparticles for Heat-Shielding Window Applications. *J. Mater. Chem. A* **2017**, *5*, 6019−6024.
(18) Zhu, M.; Song, J.; Li, T.; Gong, A.; Wang, Y.; Dai, J.; Yao, Y.; Luo, W.; Henderson, D.; Hu, L. Highly Anisotropic, Highly Transparent Wood Composites. *Adv. Mater.* **2016**, *28*, 5181−5187.
(19) Li, Y.; Fu, Q.; Yu, S.; Yan, M.; Berglund, L. Optically Transparent Wood from a Nanoporous Cellulosic Template: Combining Functional and Structural Performance. *Biomacromolecules* **2016**, *17*, 1358−1364.
(20) Yaddanapudi, H. S.; Hickerson, N.; Saini, S.; Tiwari, A. Fabrication and Characterization of Transparent Wood for Next Generation Smart Building Applications. *Vacuum* **2017**, *146*, 649−654.
(21) Li, Y.; Vasileva, E.; Sychugov, I.; Popov, S.; Berglund, L. Optically Transparent Wood: Recent Progress, Opportunities, and Challenges. *Adv. Opt. Mater.* **2018**, *6*, 1800059.
(22) Gan, W. T.; Xiao, S. L.; Gao, L. K.; Gao, R. N.; Li, J.; Zhan, X. X. Luminescent and Transparent Wood Composites Fabricated by Poly(Methyl Methacrylate) and Gamma-Fe_2O_3@YVO_4:Eu^{3+} Nanoparticle Impregnation. *ACS Sustainable Chem. Eng.* **2017**, *5*, 3855−3862.
(23) Gan, W.; Gao, L.; Xiao, S.; Zhang, W.; Zhan, X.; Li, J. Transparent Magnetic Wood Composites Based on Immobilizing Fe_3O_4 Nanoparticles into a Delignified Wood Template. *J. Mater. Sci.* **2017**, *52*, 3321−3329.
(24) Lang, A. W.; Li, Y.; De Keersmaecker, M.; Shen, D. E.; Osterholm, A. M.; Berglund, L.; Reynolds, J. R. Transparent Wood Smart Windows: Polymer Electrochromic Devices Based on Poly(3,4-Ethylenedioxythiophene):Poly(Styrene Sulfonate) Electrodes. *ChemSusChem* **2018**, *11*, 854−863.
(25) Li, Y.; Fu, Q.; Yang, X.; Berglund, L. Transparent Wood for Functional and Structural Applications. *Philos. Trans. R. Soc., A* **2018**, *376*, 20170182.
(26) Jiang, F.; Hsieh, Y.-L. Cellulose Nanocrystal Isolation from Tomato Peels and Assembled Nanofibers. *Carbohydr. Polym.* **2015**, *122*, 60−68.
(27) Saito, T.; Kimura, S.; Nishiyama, Y.; Isogai, A. Cellulose Nanofibers Prepared by Tempo-Mediated Oxidation of Native Cellulose. *Biomacromolecules* **2007**, *8*, 2485−2491.
(28) Jia, C.; Bian, H.; Gao, T.; Jiang, F.; Kierzewski, I. M.; Wang, Y.; Yao, Y.; Chen, L.; Shao, Z.; Zhu, J. Y.; Hu, L. Thermally Stable Cellulose Nanocrystals toward High-Performance 2D and 3D Nanostructures. *ACS Appl. Mater. Interfaces* **2017**, *9*, 28922−28929.
(29) Wang, R.; Chen, L.; Zhu, J. Y.; Yang, R. Tailored and Integrated Production of Carboxylated Cellulose Nanocrystals (CNC) with Nanofibrils (CNF) through Maleic Acid Hydrolysis. *ChemNanoMat* **2017**, *3*, 328−335.
(30) Zhu, H.; Parvinian, S.; Preston, C.; Vaaland, O.; Ruan, Z.; Hu, L. Transparent Nanopaper with Tailored Optical Properties. *Nanoscale* **2013**, *5*, 3787−3792.
(31) Preston, C.; Fang, Z.; Murray, J.; Zhu, H.; Dai, J.; Munday, J. N.; Hu, L. Silver Nanowire Transparent Conducting Paper-Based Electrode with High Optical Haze. *J. Mater. Chem. C* **2014**, *2*, 1248−1254.
(32) Li, Y.; Yu, S.; Veinot, J. G. C.; Linnros, J.; Berglund, L.; Sychugov, I. Luminescent Transparent Wood. *Adv. Opt. Mater.* **2017**, *5*, 1600834.
(33) Li, Y.; Yang, X.; Fu, Q.; Rojas, R.; Yan, M.; Berglund, L. Towards Centimeter Thick Transparent Wood through Interface Manipulation. *J. Mater. Chem. A* **2018**, *6*, 1094−1101.
(34) Zhu, M.; Li, T.; Davis, C. S.; Yao, Y.; Dai, J.; Wang, Y.; AlQatari, F.; Gilman, J. W.; Hu, L. Transparent and Haze Wood Composites for Highly Efficient Broadband Light Management in Solar Cells. *Nano Energy* **2016**, *26*, 332−339.
(35) Tang, Q.; Fang, L.; Wang, Y.; Zou, M.; Guo, W. Anisotropic Flexible Transparent Films from Remaining Wood Microstructures for Screen Protection and AgNW Conductive Substrate. *Nanoscale* **2018**, *10*, 4344−4353.
(36) Al-Homoud, D. M. S. Performance Characteristics and Practical Applications of Common Building Thermal Insulation Materials. *Build. Environ.* **2005**, *40*, 353−366.
(37) Papadopoulos, A. M. State of the Art in Thermal Insulation Materials and Aims for Future Developments. *Energy Build* **2005**, *37*, 77−86.
(38) Li, T.; Song, J.; Zhao, X.; Yang, Z.; Pastel, G.; Xu, S.; Jia, C.; Dai, J.; Chen, C.; Gong, A.; Jiang, F.; Yao, Y.; Fan, T.; Yang, B.; Wagberg, L.; Yang, R.; Hu, L. Anisotropic, Lightweight, Strong, and Super Thermally Insulating Nanowood with Naturally Aligned Nanocellulose. *Sci. Adv.* **2018**, *4*, No. eaar3724.
(39) Jia, C.; Li, Y.; Yang, Z.; Chen, G.; Yao, Y.; Jiang, F.; Kuang, Y.; Pastel, G.; Xie, H.; Yang, B.; Das, S.; Hu, L. Rich Mesostructures Derived from Natural Woods for Solar Steam Generation. *Joule* **2017**, *1*, 588−599.
(40) Yu, Z. T.; Xu, X.; Fan, L. W.; Hu, Y. C.; Cen, K. F. Experimental Measurements of Thermal Conductivity of Wood Species in China: Effects of Density, Temperature, and Moisture Content. *For. Prod. J.* **2011**, *61*, 130−135.
(41) Jia, C.; Jiang, F.; Hu, P.; Kuang, Y.; He, S.; Li, T.; Chen, C.; Murphy, A.; Yang, C.; Yao, Y.; Dai, J.; Raub, C. B.; Luo, X.; Hu, L. Anisotropic, Mesoporous Microfluidic Frameworks with Scalable, Aligned Cellulose Nanofibers. *ACS Appl. Mater. Interfaces* **2018**, *10*, 7362−7370.

DOI: 10.1021/acsnano.9b00089
ACS Nano 2019, 13, 9993−10001

(42) Jia, C.; Chen, L.; Shao, Z.; Agarwal, U. P.; Hu, L.; Zhu, J. Y. Using a Fully Recyclable Dicarboxylic Acid for Producing Dispersible and Thermally Stable Cellulose Nanomaterials from Different Cellulosic Sources. *Cellulose* **2017**, *24*, 2483−2498.
(43) Jia, C.; Li, T.; Chen, C.; Dai, J.; Kierzewski, I. M.; Song, J.; Li, Y.; Yang, C.; Wang, C.; Hu, L. Scalable, Anisotropic Transparent Paper Directly from Wood for Light Management in Solar Cells. *Nano Energy* **2017**, *36*, 366−373.

DOI: 10.1021/acsnano.9b00089
ACS Nano 2019, 13, 9993−10001